

Comparative Analysis of Mononuclear 1:1 and 2:1 Tetravalent Actinide (U, Th, Np) Complexes: Crystal Structure, Spectroscopy, and Electrochemistry

Bansal, D.; Kaden, P.; Patzschke, M.; März, J.; Schmidt, M.;

Originally published:

June 2022

Inorganic Chemistry 61(2022)27, 10509-10520

DOI: <https://doi.org/10.1021/acs.inorgchem.2c01405>

Perma-Link to Publication Repository of HZDR:

<https://www.hzdr.de/publications/Publ-34786>

Release of the secondary publication
on the basis of the German Copyright Law § 38 Section 4.

Comparative Analysis of Mononuclear 1:1 and 2:1 Tetravalent Actinide (U, Th, Np) Complexes: Crystal Structure, Spectroscopy, and Electrochemistry

Deepak Bansal, Peter Kaden, Michael Patzschke, Juliane März, and Moritz Schmidt**

Institute of Resource Ecology, Helmholtz-Zentrum Dresden-Rossendorf, Bautzner Landstraße
400, 01328 Dresden, Germany

ABSTRACT. Six mononuclear tetravalent actinide complexes (**1-6**) have been synthesized using a new Schiff base ligand 2-methoxy-6-(((2-methyl-1-(pyridin-2-yl)propyl)imino)methyl)phenol (**HL^{Pr}**). The **HL^{Pr}** is treated with tetravalent actinide elements in varied stoichiometry to afford mononuclear 1:1 complexes [$\text{MCl}_3\text{-L}^{\text{Pr}}\cdot n\text{THF}$] (**1-3**) and 2:1 complexes [$\text{MCl}_2\text{-L}^{\text{Pr}}_2$] (**4-6**) ($\text{M} = \text{Th}^{4+}$ (**1** and **4**), U^{4+} (**2** and **5**) and Np^{4+} (**3** and **6**)). All complexes are characterized using different analytical techniques such as IR, NMR, and absorption spectroscopy as well as crystallography. UV-vis spectroscopy revealed more red-shifted absorption spectra for 2:1 complexes as compared to 1:1 complexes. ^1H NMR of Th(IV) complexes exhibit diamagnetic spectra whereas U(IV) and Np(IV) complexes revealed paramagnetically shifted ^1H NMR. Interestingly, NMR signals are paramagnetically shifted between -70 to 40 ppm in **2** and **3**, but are confined within -35 to 25 ppm in 2:1 complexes **5** and **6**. Single crystal structures for 1:1 complexes revealed an eight-coordinated Th(IV) complex (**1**) and seven-coordinated U(IV) (**2**) and Np(IV) (**3**) complexes. Whereas, all 2:1 complexes **4-6** were isolated as eight-coordinated isostructural molecules. The geometry around the Th^{4+} center in **1** is found to be trigonal dodecahedral and, capped trigonal prismatic around

U(IV) and Np(IV) centers in **2** and **3**, respectively. Whereas, An^{4+} centers in 2:1 complexes are present in dodecahedral geometry. Importantly, 2:1 complexes exhibit increased bond distances in comparison to their 1:1 counterparts as well as interesting bond modulation w.r.t. ionic radii of An(IV) centers. Cyclic voltammetry displays an increased oxidation potential of the ligand by 300 to 500 mV, after coordination with An^{4+} . CV studies indicates Th(IV)/Th(II) reduction beyond -2.3 V whereas attempts were made to identify redox potentials for U(IV) and Np(IV) centers. Spectroscopic binding studies reveal that complex stability in 1:1 stoichiometry follows the order $Th^{4+} \approx U^{4+} > Np^{4+}$.

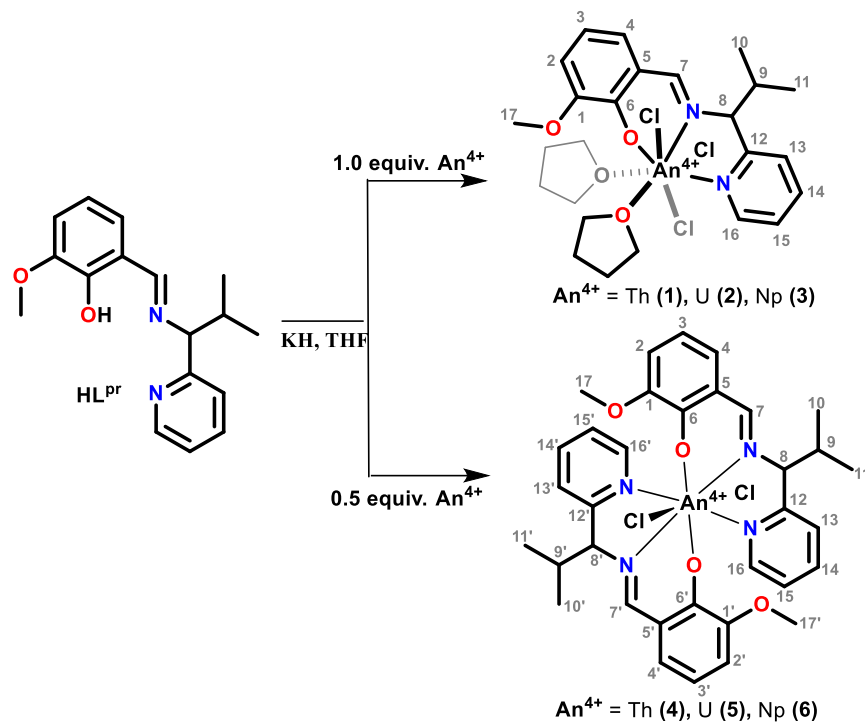
Introduction

In recent years, coordination chemistry of actinide elements has gained widespread attention due to their underexplored coordination properties as well as interesting redox and catalytic properties. [1-14] Importantly, studies on actinide chemistry mostly focus on uranyl $U(VI)O_2^{2+}$, with significantly fewer studies for any other actinide or oxidation state.[15-21] Nowadays, efforts are underway to synthesize and isolate highly reactive low valent actinide compounds, after the realization of their potential in small molecule activation and catalysis.[4,22-25] Meanwhile, the low valent actinide complexes are dominated by cyclopentadienyl and related ligands, emphasizing a demand to design and synthesize other organic ligand(s) to stabilize low valent actinide complexes.[6,15,26,27] In this context, di- and mono-anionic Schiff base ligands are frequently explored due to the presence of a strongly coordinating aryl-oxide donor along with chelating motif. While multiple $U(VI)O_2^{2+}$, U(IV), and Th(IV), and fewer Np(IV) complexes have been reported with di-anionic Schiff base ligands, e.g. of salen-type [5,21,28-33], Uranium complexes with Schiff base ligands have been shown to promote interesting electrochemical

processes owing to the non-innocent redox behavior of the ligand(s).[3-5] Therefore, there is a need for the in-depth characterization of structure, bond properties, and redox behavior of actinide complexes with non-redox innocent ligands to achieve actinide complexes of desired properties.

Concerning the relatively well-explored dianionic Schiff base ligands, there are no reports on the isolation of mononuclear 1:1 actinide complex(es) with monoanionic Schiff base ligands. Notably, monoanionic, tridentate Schiff base ligands are promising candidates to produce 1:1 actinide complex with larger numbers of labile sites and thus potentially more versatile reactivity.[34,35] Indeed, synthesis and isolation of 1:1 Schiff base-actinide complexes requires careful control of the synthesis conditions due to the potential formation of dimerized products or other unintended follow-up reactions.[36] Therefore, mono-anionic Schiff base ligands are largely reported as stable bis-actinide complexes.[33,36] On the other hand, availability of such 1:1 actinide complex will be extremely informative for comparative analysis of coordination, structural and electronic variations between mono- (1:1) and bis-ligated (2:1) An complexes.

Taking this into consideration we have synthesized a new non-redox-innocent mono-ionic Schiff base ligand **HL^{Pr}** and its mono-ligated (**1-3**) and bis-ligated (**4-6**) actinide complexes [AnCl_x-(**L^{Pr}**)_y·nTHF] (An = Th (**1** and **4**), U (**2** and **5**) and Np (**3** and **6**); x = 3, y = n = 1 for **1-3**, except n = 2 for **1**; x = y = 2 and n = 0 for **4-6** complexes) (Scheme 1). All complexes were comprehensively characterized by FTIR, UV-vis, NMR, SC-XRD, and cyclic voltammetry to understand the influence of structure and electronic properties on bonding, coordination, and redox behavior.



Scheme 1. Synthetic route for the preparation of actinide complexes **1-6** with **HL^{Pr}**.

Experimental

Caution!

Th-232sec, U-nat and Np-237+ consist of long lived α emitters with half-lives of 1.41×10^{10} , 4.47×10^9 and 2.14×10^6 years, respectively. Special precautions as well as appropriate equipment and facilities for radiation protection are required for handling these materials. All experiments were carried out in a controlled laboratory at the Institute of Resource Ecology, Helmholtz-Zentrum Dresden-Rossendorf.

General remarks

All preparations were performed under the rigorous exclusion of moisture and oxygen in nitrogen filled glove boxes or using Schlenk techniques. The used solvents were dried using solvent

purification system MBraun SPS 5 and stored over molecular sieve (3 Å) prior to use. Chemicals were sourced from Sigma-Aldrich and were used as received. Thin layer chromatography (TLC) was carried out on aluminum plates coated with silica gel mixed with fluorescent indicator sourced from Merck, Germany. NMR spectra were recorded inside a controlled laboratory on a Varian Inova 400 spectrometer with an ATB indirect probe equipped with z-gradients operating at a ^1H frequency of 399.89 MHz and a ^{13}C frequency of 100.56 MHz. Special precautions were taken to avoid contamination. All spectra were recorded with a Varian AutoX ID probe head with z gradient. Deuterated solvents were purchased at Deutero GmbH and dried over potassium mirror prior to use. FTIR spectra were measured on an Agilent Cary 630 FT-IR spectrometer equipped with a single-reflection attenuated total reflection (ATR) accessory made of diamond. The measurements were performed in an inert glove box filled with N_2 . The spectra were recorded between 4000 and 650 cm^{-1} with a resolution of 2 cm^{-1} . UV/visible/NIR spectra were recorded with a J&M Analytik AG TIDAS 100 spectrometer connected with optical fibers to a cuvette housing in the glove box. The spectra were recorded between 200 and 1025 nm in 1 cm quartz cuvettes.

Cyclic and Differential Pulse Voltammetry (CV/DPV): CV and DPV were carried out using a computer controlled potentiostat (CHI 650C), and a standard three electrode arrangement that consisted of glassy carbon, platinum, and saturated calomel (SCE) containing Ag/AgCl in AgNO_3 acetonitrile solution as working, auxiliary, and reference electrodes, respectively.[37,38] All electrochemical measurements were carried out in dry and Ar-purged acetonitrile with $n\text{-Bu}_4\text{NPF}_6$ as the supporting electrolyte. All the potentials are calculated in reference to $\text{Fc}^{0/+}$ which was measured separately.

X-ray Crystallography: The data for **1-6** were analyzed on a Bruker D8 Venture single-crystal X-ray diffractometer with micro-focused Mo K α radiation ($\lambda = 0.71073$ Å) and a PHOTON 100 CMOS detector. The frames for **1**, **2**, and **4-6** were collected at 100 K, and for **3** at 293 K. Data treatment was performed with the Bruker APEX 3 program suite including the Bruker SAINT software package for integration [39], and empirical absorption corrections was applied by using the spherical harmonic incorporated in the SCALE3 ABSPACK scaling algorithm.[40] The structures were solved and refined with full-matrix least-squares data on F^2 using the Bruker SHELXTL [41] software package and SHELXL-2018 [42] in the WinGX module. [43] All hydrogen atoms were fixed at the calculated positions and refined isotropically. Complex **2** exhibits a Flack parameter of 0.380 suggesting potential racemization. [45] For complexes **4** and **6**, some electron density, potentially corresponding to disordered THF or toluene molecules, could not be resolved and was therefore masked using the solvent masking ‘Squeeze’ command in PLATON. [44] In complex **5**, highly disordered toluene molecules are modelled using OLEX 2 software. Details of the crystallographic data collection and structural solution parameters are provided in Table S1.

Synthesis

2-methoxy-6-(((2-methyl-1-(pyridin-2-yl)propyl)imino)methyl) phenol (HL^{Pr}). In a 25 ml round bottom flask, 2-methyl-1-(pyridin-2-yl)propan-1-amine dihydrochloride (0.17 g, 0.78 mmol) was dissolved in deionized water (5ml) and neutralized by solid Na₂CO₃ (0.2 g, 1.95 mmol). The solution was stirred for 20 minutes followed by the dropwise addition of methanolic solution of o-vanillin (0.1 g, 0.65 mmol) resulting in a yellow color solution. The reaction was further stirred for another 30 minutes resulting in the formation of the yellow oily product. The reaction was stopped and dichloromethane (25 ml) was added to the reaction mixture dissolving the oily

product. The yellow colored organic layer was isolated using a separating funnel. The organic portion was washed multiple times with water followed by removal of DCM under reduced pressure to afford an oily product. Yield = 96% (179 mg). ^1H NMR (400 MHz, CDCl_3): δ = 14.13 (d, 1H, $-(\text{H})\text{C}=\text{N}$), 8.39 (s, 1H, $-\text{CH}_{\text{py}}$), 7.67 (m, 1H, $-\text{CH}_{\text{py}}$), 7.41 (d, 1H, $-\text{CH}_{\text{phenoxide}}$), 7.18 (m, 1H, $-\text{CH}_{\text{py}}$), 6.91-6.88 (m, 2H, $-\text{CH}_{\text{py}}$ & $-\text{CH}_{\text{phenoxide}}$), 6.78 (t, 1H, $-\text{CH}_{\text{phenoxide}}$), 4.32 (d, 1H, $-(\text{H})\text{CCH}(\text{CH}_3)_2$), 3.87 (s, 3H, $-\text{OCH}_3$), 2.39 (m, 1H, $-\text{HC}(\text{CH}_3)_2$), 0.87 (d, 6H, $-\text{CH}_3$). ^{13}C NMR (125 MHz, CDCl_3): δ = 165.45, 161.07, 151.71, 148.71, 148.38, 137.09, 124.46, 123.05, 122.34, 121.88, 118.39, 113.99, 80.80, 55.99, 34.30, 19.72, 17.67. FTIR spectrum (ATR, selected peaks, cm^{-1}): 1626 ($\text{C}=\text{N}$), 1586 ($\text{C}=\text{N}_{\text{py}}$). Absorption spectrum [λ_{max} , nm, THF]: 334, 440.

[ThCl₃-L^{pr}.2THF] (**1**). To a scintillation vial, charged with 1 ml solution of **HL^{pr}** (0.02g, 0.070 mmol) in dry THF, was added with excess of KH, leading to the immediate evolution of molecular hydrogen gas. The reaction mixture was stirred for 15 min and the clear supernatant liquid was separated from unreacted solid KH by centrifugation. To a clear supernatant solution, $\text{ThCl}_4 \cdot 2\text{DME}$ (0.038g, 0.070 mmol) solution in dry THF (1ml) was added dropwise under constant stirring resulting in formation of yellow solution. The reaction mixture was stirred for another 1h and was centrifuged to remove salt impurity. The resulting yellow color solution was left for evaporation to afford deposition of crystalline material at the bottom of vial. Yield = 86% (41 mg). Anal. calc. for $\text{C}_{25}\text{H}_{35}\text{Cl}_3\text{N}_2\text{O}_4\text{Th}$: C, 37.42; H, 4.57; N, 3.45. Found: C, 39.20; H, 4.61; N, 3.66. ^1H NMR (400 MHz, $\text{THF}-d_8$): δ = 9.95 (d, 1H), 8.44 (s, 1H), 7.89 (t, 1H), 7.46 (d, 1H), 7.40 (t, 1H), 7.08 (m, 1H), 7.00 (d, 1H), 6.74 (t, 1H), 4.43 (m, 1H), 3.78 (s, 3H), 3.32 (m, 1H), 0.92-0.85 (dd, 6H). ^{13}C NMR (125 MHz, $\text{THF}-d_8$): δ = 168.48, 162.24, 153.21, 150.41, 138.91, 127.29, 124.80, 123.47, 118.51, 116.53, 88.86, 55.67, 34.56. FTIR spectrum (ATR, selected peaks, cm^{-1}): 1612 ($\text{C}=\text{N}$), 1559 ($\text{C}=\text{N}_{\text{py}}$). Absorption spectrum [λ_{max} , nm, THF]: 305, 370, 430.

[UCl_3 - L^{Pr} -THF] (**2**). The synthesis of **2** was performed in the similar manner to **1** except using UCl_4 (0.026 g, 0.070 mmol) as the uranium precursor. After the dropwise addition of UCl_4 solution, the reaction was stirred for 30 min followed by centrifugation to remove insoluble salt impurities. The resulting green colour solution was diffused with toluene to afford green crystal after 72 h. Yield = 83% (41 mg). Anal. calc. for $C_{21}H_{27}Cl_3N_2O_3U \cdot 2THF$: C, 38.90; H, 4.57; N, 3.63. Found: C, 37.0; H, 3.89; N, 3.59. 1H NMR (400 MHz, THF- d_8): δ = 38.45 (s, 1H), 36.48 (s, 1H), 35.90 (s, 1H), 31.87 (s, 1H), 23.87 (s, 1H), 20.11 (s, 3H), 3.19 (s, 1H), 0.94 (s, 1H), -0.27 (s, 1H), -15.43 (s, 3H), -15.57 (s, 1H), -24.69 (s, 3H), -29.23 (s, 1H), -71.67 (s, 1H). FTIR spectrum (ATR, selected peaks, cm^{-1}): 1612 (C=N), 1563 (C=N_{py}). Absorption spectrum [λ_{max} , nm, THF]: 309, 370, 470.

[$NpCl_3$ - L^{Pr} -THF] (**3**). The synthesis of **3** was performed in the similar manner to **1** using $NpCl_4 \cdot 2DME$ (0.029g, 0.070 mmol) as the neptunium precursor. The dropwise addition of Np^{4+} solution resulted in the formation of brown color solution. Crystal suitable for X-ray diffraction were obtained by diffusing pentane to the complex solution in THF to afford dark brown crystals within 24h. Yield = 85% (42 mg). 1H NMR (400 MHz, THF- d_8): δ = 41.37 (s, 1H), 37.48 (s, 1H), 35.12 (s, 1H), 27.19 (s, 1H), 21.44 (s, 1H), 16.23 (s, 3H), 5.02 (s, 1H), 0.31 (s, 1H), -15.51 (s, 4H), -20.14 (s, 3H), -30.54 (s, 1H), -65.23 (s, 1H). FTIR spectrum (ATR, selected peaks, cm^{-1}): 1613(C=N), 1559 (C=N_{py}). Absorption spectrum [λ_{max} , nm, THF]: 373, 474.

[$ThCl_2$ -(L^{Pr})₂] (**4**). The synthesis of **4** was performed in the similar manner to **1** using 0.5 equiv. $ThCl_4 \cdot 2DME$ (0.015g, 0.035 mmol) as the Thorium precursor. The dropwise addition of Th^{4+} solution resulted in the formation of colorless solution. Crystal suitable for X-ray diffraction were obtained by diffusing pentane to the complex solution in THF to afford colorless crystals within 24h. Yield = 83% (51 mg). Anal. calc. for $C_{34}H_{38}Cl_2N_4O_4Th$: C, 46.96; H, 4.40; N, 6.44. Found:

165 C, 46.25; H, 4.18; N, 6.72. ^1H NMR (400 MHz, THF- d_8): δ = 9.66 (s, 2H), 8.49 (s, 2H), 7.98 (s,
166 2H), 7.60 (s, 2H), 7.41 (s, 2H), 7.0 (s, 4H), 6.71 (s, 2H), 4.50 (s, 2H), 3.75 (s, 2H), 3.39 (s, 6H),
167 0.88 (s, 12H). FTIR spectrum (ATR, selected peaks, cm^{-1}): 1610($\text{C}=\text{N}_{\text{py}}$), 1551 ($\text{C}=\text{N}$). Absorption
168 spectrum [λ_{max} , nm, THF]: 442.

169 $[\text{UCl}_2-(\text{L}^{\text{Pr}})_2]$ (**5**). The synthesis of **5** was performed in the similar manner to **2** except using 0.5
170 equiv. UCl_4 (0.013 g, 0.035 mmol) as the uranium precursor. The dropwise addition of U^{4+}
171 solution resulted in the formation of brown solution. The solvent was removed under reduced
172 pressure and the resulting solid compound was washed with pentane to afford brown precipitates.
173 The precipitates were redissolved in toluene followed by diffusion with pentane to afford brown
174 crystals after 48 h. Yield = 80% (49 mg). Anal. calc. for $\text{C}_{34}\text{H}_{38}\text{Cl}_2\text{N}_4\text{O}_4\text{U}$: C, 46.64; H, 4.37; N,
175 6.40. Found: C, 46.94; H, 4.82; N, 6.59. ^1H NMR (400 MHz, THF- d_8): δ = 23.93 (s, 1H), 21.40
176 (s, 1H), 15.95 (s, 1H), 15.26 (s, 1H), 14.66 (s, 1H), 13.96 (s, 1H), 12.89 (s, 1H), 12.78 (s, 1H),
177 12.28 (s, 1H), 11.68 (s, 3H), 10.03 (s, 3H), 2.24 (s, 3H), 1.02 (s, 3H), 0.38 (s, 1H), -0.61 (s, 1H), -
178 1.26 (s, 1H), -5.11 (s, 3H), -10.73 (s, 3H), -11.34 (s, 3H), -13.84 (s, 1H), -14.0 (s, 1H), -14.60 (s,
179 3H), -23.89 (s, 1H), -26.80 (s, 1H), -29.93 (s, 1H), -33.40 (s, 1H). FTIR spectrum (ATR, selected
180 peaks, cm^{-1}): 1613 ($\text{C}=\text{N}_{\text{py}}$), 1560 ($\text{C}=\text{N}$). Absorption spectrum [λ_{max} , nm, THF]: 442, 523.

181 $[\text{NpCl}_2-(\text{L}^{\text{Pr}})_2]$ (**6**). The synthesis of **6** was performed in the similar manner to **5** using 0.5 equiv.
182 $\text{NpCl}_4 \cdot 2\text{DME}$ (0.015 g, 0.035 mmol) as the neptunium precursor to afford wine-red colored
183 complex solution. Crystals suitable for X-ray diffraction were obtained in a similar manner like **5**.
184 Yield = 84% (45 mg). ^1H NMR (400 MHz, THF- d_8): δ = 22.37 (s, 1H), 18.32 (s, 1H), 16.46 (s,
185 1H), 15.25 (s, 1H), 14.79 (s, 1H), 13.04 (s, 3H), 11.52 (s, 3H), 10.99 (s, 1H), 10.24 (s, 1H), 9.21
186 (s, 1H), 8.49 (s, 1H), 1.86 (s, 3H), 1.28 (s, 1H), 0.85 (s, 1H), 0.51 (s, 1H), -0.46 (s, 1H), -6.26 (s,
187 3H), -9.85 (s, 3H), -10.54 (s, 1H), -11.65 (s, 1H), -12.26 (s, 3H), -13.31 (s, 3H), -21.21 (s, 1H), -

22.86 (s, 1H), -26.39 (s, 1H), -28.77 (s, 1H). FTIR spectrum (ATR, selected peaks, cm^{-1}):
1613($\text{C}=\text{N}_{\text{py}}$), 1551 ($\text{C}=\text{N}$). Absorption spectrum [λ_{max} , nm, THF]: 452, 530.

Results and discussion

Condensation of o-vanillin with 2-methyl-1-(pyridine-2-yl)propane-1-amine dihydrochloride results in the isolation of a yellow oily product **HL^{Pr}** in high yield. The formation of **HL^{Pr}** was confirmed by the presence of the characteristic (H)C=N proton signal at 8.51 ppm in ^1H NMR (Figure S1, ESI). Complexes **1-6** were synthesized by treating (**L^{Pr}**)⁻, deprotonated with KH, with An^{4+} (An = Th, U, Np) to afford mononuclear 1:1 (**1-3**) and 2:1 (**4-6**) complexes. Interestingly, addition of Th^{4+} or U^{4+} in different stoichiometry leads to the observation of differently colored solutions during the preparation of 1:1 and 2:1 complexes (see experimental section for detail). FT-IR measurements exhibit superimposable spectra of all the complexes suggesting the coordination of metal ions with the ligand in a similar fashion (Figure S2). All complexes exhibit (H)C=N $\nu_{\text{C}=\text{N}}$ and pyridyl $\nu_{\text{C}=\text{N}}$ stretching modes as expected, bathochromically shifted by 14 cm^{-1} and $23\text{-}31\text{ cm}^{-1}$ in relation to **HL^{Pr}**, respectively, indicating a complexation involving (H)C=N and pyridyl nitrogen atoms (Table 1). M-Cl bond vibrations appear below 650 cm^{-1} and thus could not be identified. [46] The absorption spectrum of the ligand **HL^{Pr}** exhibits an absorption maximum at approx. 334 nm (λ_{max}) along with a weak band at 440 nm (Figure S3). This ligand-based absorption feature at 334 nm (in **HL^{Pr}**) is red shifted by 30-40 nm in 1:1 complexes **1-3**, whereas it is red shifted by 110-120 nm for the 2:1 complexes **4-6**. Moreover, weak absorption bands between 580 and 1025 nm, indicating $f\text{-}f$ transitions, are observed for complexes **2, 3, 5, and 6** (Figure S3). [45]

Table 1. Absorbance and selected IR stretches in **HL^{pr}** and complexes **1-6**.

	HL^{pr}	1	2	3	4	5	6
Absorbance (nm)							
	334, 440	366,	370, 473	370, 490	442	442	452
		436,				523	530
FTIR vibrations (cm ⁻¹)							
$\nu_{C=N}$ (HC=N)	1586	1563	1563	1559	1551	1560	1551
$\nu_{C=N}$ (pyridyl)	1626	1612	1612	1613	1610	1613	1613

210 NMR Spectroscopy

211 To analyze the molecular structure in solution, NMR spectroscopy was used for all complexes
 212 (Figures S4-S12). Complexes **1** and **4** exhibit diamagnetically shifted ¹H NMR spectra, whereas
 213 highly shifted paramagnetic ¹H NMR spectra were observed for complexes **2**, **3**, **5**, and **6** (Table
 214 2). The proton signals in **1** and **4** were observed downfield shifted as compared to free ligand
 215 (Figures S4 and S8). Interestingly, the change of coordination environment around the An center
 216 from 1:1 to 2:1 complex exhibits small but distinct shifts of these diamagnetic ¹H NMR signals.
 217 For example, the (H7)C=N proton signal in 2:1 complex **4** is comparatively more upfield shifted
 218 by 0.30 ppm than in 1:1 complex **1**. Whereas, proton signals for (H8)C and (H9)C in **4** are
 219 downfield shifted by 0.07 ppm and 0.33 ppm respectively, as compared to their 1:1 counterparts.
 220 Apart from that, pyridyl protons appear between 6.71 ppm to 7.97 ppm for both complexes, **1** and
 221 **4**. We believe that the presence of the additional ligand results in a reduced interaction of Th(IV)
 222 with both ligands leading to the upfield shift in the proton signals in **4**. On the other hand, we
 223 observe the presence of additional NMR signals corresponding to every ¹H signal in both **1** and **4**.
 224 Since we worked with the ligand having both ‘R’ and ‘S’ configuration at C8 center, we tentatively

assign these signals as belonging to the complex moiety with the ligand in the opposite configuration. Based on integration of both types of NMR signals, we can estimate an enantiomeric excess for one of the conformations by ~50% in our starting material.

Due to the presence of unpaired $5f$ electrons in U(IV) and Np(IV), complexes **2**, **3**, **5**, and **6** exhibit paramagnetically shifted ^1H NMR signals (Figures S5, S9 and S10). Notably, unpaired electron density mainly interacts with the NMR observed nuclear spins either due to spin dipolar interactions in form of pseudo contact shifts (PCS) or by Fermi contact interactions (FCS) which may arise from molecular orbitals (MO) containing unpaired electron density originating from metal contributions to the MO and featuring significant levels of s -contribution at the observed nucleus. Typically, only sizeable PCS contributions are detected on nuclei remote from the metal center. From previous studies, a prolate density of unpaired electrons is expected at the An^{4+} centers [28-30, 45, 47-49]. This results in a PCS field that leads to shielding PCS shifts in the direction of the z -axis of the magnetic tensor and to de-shielding PCS shifts in the x,y -plane. Thus nuclei with resonances found in the negative scale are expected to be located in z -direction relative to the metal center and those found shifted to positive ppm values are expected close to the x,y -plane. Apart from that, the change in coordination environment from 1:1 to 2:1 around An^{4+} center is also very prominent in the paramagnetically shifted NMR. [50] Interestingly, Np(IV) complexes **3** and **6** exhibit similar NMR patterns as their U(IV) counterparts **2** and **5**, respectively. Moreover, the 1:1 Np(IV) complex **3** is paramagnetically more shifted as compared to its U(IV) counterpart **2** whereas, in contrast, 2:1 U(IV) complex **5** is comparatively more shifted than its Np(IV) counterpart **6** (see Table 2). The ^1H NMR signals for 1:1 complexes **2** and **3** appear in the range between -70 to 40 ppm, whereas these signals are confined within -35 to 25 ppm for 2:1 complexes **5** and **6** (Figure 1).

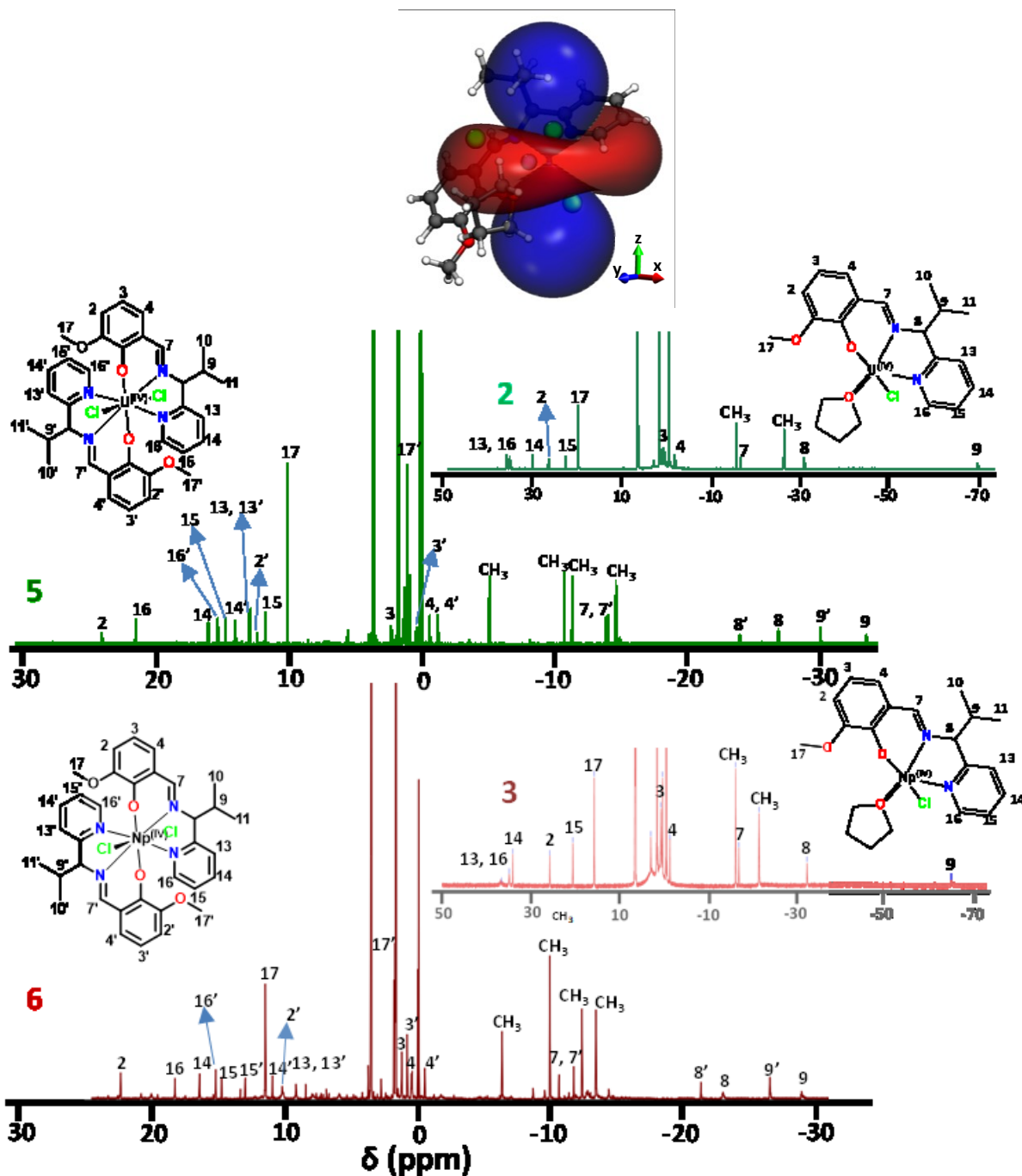


Figure 1. Comparative ^1H NMR spectra for 1:1 complexes **2** and **3** and 2:1 complexes **5** and **6**. A schematic representation of possible PCS cones is shown at the top for the 1:1 complex. The corresponding figure for the 2:1 complexes is discussed in the SI.

252 Notably, while complexes **2** and **3** exhibit six signals on the negative side and seven signals on the
253 positive side of the spectra, complexes **5** and **6** display twice the number of signals on the same
254 side of spectrum, due to the presence of two enantiomers of the ligand. More importantly, proton
255 signals (H and H') for both ligands in the 2:1 complexes exhibit distinct positions suggesting
256 different electronic interactions of each ligand with the An^{4+} center.[50] The highly shifted
257 isopropyl 'H9' proton at -69.74 ppm is found for the 1:1 U(IV) complex **2** whereas, in 2:1 U(IV)
258 complex **5**, H9 and H9' protons appear separately at -33.40 ppm and -29.93 ppm, respectively.
259 These values are shifted by approximately 35 to 40 ppm when changing from 1:1 to 2:1 complexes.
260 The paramagnetic shift is considerably reduced to 5-10 ppm for H8 (-26.78 ppm) and H8'
261 (-23.89 ppm) protons in **5** as compared to its position in **2** (-30.59 ppm). The resonances of the
262 whole isopropyl group appear in the strongly shielded region of the NMR spectrum and thus should
263 be located in the z-axis region of the PCS field. [51] In contrast, the pyridyl proton 'H13' in **2** is
264 observed as most downfield shifted signal at 36.45 ppm, while a phenoxide 'H2' (23.90 ppm) from
265 one of the ligands, was found to be the most de-shielded proton in **5**. Moreover, phenoxide protons
266 (H2, H3/H3', H4/H4') are shifted to the similar extent in both the complexes **2** and **5**, except H2'
267 (12.27 ppm) in **5**, which appeared highly shielded as compared to H2 (27.16 ppm) in complex **2**.
268 This indicates that these nuclei and thus the respective aromatic rings are located in the x,y-plane
269 of the PCS field. Variations of the magnitude of shielding in the respective resonances may account
270 for slight differences in position in the PCS field or originate from FCS contributions due to the
271 differences in the respective interactions of the donors with the metal center. Both PCS and FCS
272 are strongly influenced by the coordination geometry around the metal center and thus depend on
273 the size of the metal center itself. In conclusion, we observe a quite symmetric complexation in
274 the 2:1 ligands that resembles the coordination environment in the 1:1 complexes, with the ligands

275 having coordinating heteroaromatic rings in the x,y-plane region and the isopropyl groups in the
 276 z-direction (magnetic principal axis) of the PCS field. Due to the observed one coordination
 277 environment in the 1:1 complexes and two sets of resonances in the 2:1 complexes, most likely
 278 due to the presences of both enantiomers of the ligand, we assume that in the time and ensemble
 279 average of the NMR spectra, we only observe a single (averaged) coordination environment. In
 280 case of the 2:1 complexes, the magnetic principal axis coincides with a (pseudo-) symmetry axis,
 281 most likely coinciding with the O-U-O bond. It is evident from the NMR spectra that the structure
 282 of the 2:1 complexes in solution differs from that found in the solid state (see below). Assigning
 283 magnetic axes or even “PCS cones” to the molecule is further complicated by the molecules’ low
 284 symmetry, which causes all three quadrupole moments to be unequal. Details regarding this
 285 assignment can be found in the SI.

Table 2. Selected ^1H NMR shift (ppm) for complexes **1-6**.

Proton	HL ^{pr}	1	2	3	4	5	6
2	6.86	6.99	27.16	27.26	7.0	23.90, 12.27	22.37, 10.24
3	6.74	6.74	1.10	2.05	6.71	2.245, 0.38	1.28, 0.85
4	7.49	7.46	-1.35	0.31	7.60	-0.63, -1.24	0.51, -0.46
7	8.52	9.95	-16.26	-16.45	9.66	-14.0, -13.86	-10.54, -11.65
8	4.32	4.43	-30.59	-31.90	4.50	-26.78, -23.89	-22.86, -21.20
9	2.39	3.32	-69.74	-64.66	3.75	-33.39, -29.93	-28.77, -26.39
10, 11	0.87	0.92-0.85	-15.29, -25.99	-15.72, -21.02	0.88	-14.60, -11.33, -10.72, -5.11	-13.31, -12.26, -9.85, -6.26
13	6.89	7.08	36.45	41.37	7.0	12.79, 12.91	9.21, 8.49
14	7.65	7.89	30.73	35.23	7.98	15.96, 13.96	10.99, 16.46

15	7.15	7.39	23.29	21.49	7.41	14.65, 11.67	14.79, 13.04	286
16	8.39	8.44	35.81	37.38	8.49	21.40, 15.27	18.32, 15.25	
17	3.85	3.78	20.40	16.27	3.39	10.03, 1.02	11.52, 1.86	

Molecular structures of 1-6

All complexes have been characterized crystallographically and exhibit mononuclear molecular structures with 1:1 and 2:1 L:An stoichiometry for **1-3** and **4-6**, respectively. The isolated complexes were found with the chemical compositions $[\text{AnCl}_3\text{L}^{\text{Pr}}\cdot(\text{THF})_n]$ for **1-3** and $[\text{AnCl}_2\text{L}^{\text{Pr}}_2]$ for **4-6** [An = Th, U and Np; n = 1 or 2] (Figures 2 and 3, and Table 3). Complexes **1-3** contain one ligand unit, three chlorine atoms and one or two THF molecule(s) within their coordination sphere. Whereas 2:1 complexes **4-6** were isolated as isostructural eight-coordinated tetravalent complexes containing two ligand units and two chloride ions. The crystal structures of **2** and **3** exhibit seven-coordinated U^{4+} and Np^{4+} centers coordinated by the ligand via phenoxide oxygen (O_{Ph}), imine nitrogen ($\text{N}_{\text{C}=\text{N}}$), pyridyl nitrogen (N_{py}), as well as three chloride ions and a THF molecule. However, complex **1** exhibits an eight-coordinated Th^{4+} due to the presence of an additionally coordinated THF molecule. The geometry around the U^{4+} and Np^{4+} center in **2** and **3** can be best described as capped trigonal prismatic with distortion of 6.96 % and 13.968 % respectively (Figure 2 inset and Table S3).[52] In **1**, however, an additionally coordinating THF molecule results in the formation of an eight-coordinated trigonal dodecahedral geometry (distortion = 5.92 %) around the Th^{4+} center (Figure 2, Inset). Gratifyingly, all the 2:1 complexes **4-6** were found having a dodecahedral geometry around the An(IV) centers deviating by 5.62 %, 5.46 % and 5.12 %, respectively (see Table S3).

The An– O_{Ph} , An– $\text{N}_{\text{C}=\text{N}}$, An– N_{py} and An–Cl bond distances were found to be in the range 2.199–2.234 Å, 2.518–2.673 Å, 2.559–2.640 Å and 2.626–2.734 Å, respectively for complexes **1-3**, and

2.235–2.167 Å, 2.653–2.615 Å, 2.743–2.669 Å and 2.681–2.766 Å, respectively for complexes **4**–**6** (Table 3). The An–O_{Ph} and An–N_{C=N} distances in the 2:1 complexes **4**–**6** are comparable with previously reported An(IV) complexes, while bond distances for 1:1 complexes **1**–**3** are comparatively shorter by approximately 0.5 Å (Table S2). Interestingly, the bond distances in bis-ligated complexes **4**–**6** are larger as compared to their 1:1 counterpart **1**–**3**, except for Th–N_{C=N} in **4** (2.653 Å) which is shorter by 0.02 Å than Th–N_{C=N} in **1** (2.673 Å), potentially due to the presence of an additional THF molecule in **1**. Notably, comparative analysis of mono-ligated complex **1** with bis-ligated complexes **4** exhibit marginal change of approximately 0.03 Å for Th–O_{Ph}, Th–N_{C=N}, Th–N_{py} and Th–Cl. Whereas U(IV) and Np(IV) complexes **5** and **6** exhibit considerably larger increases of nearly 0.05 Å (An–O_{Ph}), 0.08 Å (An–N_{C=N}), 0.12 Å (An–N_{py}) and 0.07 Å (An–Cl) as compared to their 1:1 counterpart **2** and **3**. These values indicate a weakening of An–ligand interactions in 2:1 complexes as compared to the 1:1 complexes. Moreover, bond distance comparison among 1:1 complexes **1**–**3** and 2:1 complexes **4**–**6** exhibits largest changes from Th(IV) (**1**/**4**) to U(IV) (**2**/**5**), with noticeable decreases in An–O_{Ph}, An–N_{C=N} and An–N_{py} distances by -0.07 Å, 0.15 Å and 0.12 Å, respectively from **1** to **2**, and by 0.06 Å, 0.05 Å, and 0.02 Å, respectively from **4** to **5**. Similarly, An–Cl bond distances also exhibit decreases of 0.08–0.10 Å from **1** to **2** and 0.06 Å from **4** to **5**, while no considerable change in bond distances is observed among U to Np complexes. Such a trend in decreasing bond distances from Th⁴⁺ (0.94 Å) > U⁴⁺ (0.89 Å) > Np⁴⁺ (0.87 Å) while traversing the An series is well describe in literature. [29] Interestingly, the 1:1 complexes exhibit more pronounced decreases in An–N_{C=N/py} bond distances as compared to An–O_{Ph} suggesting a potential covalent contribution in An–N bonds which is not present in An–O_{Ph}.

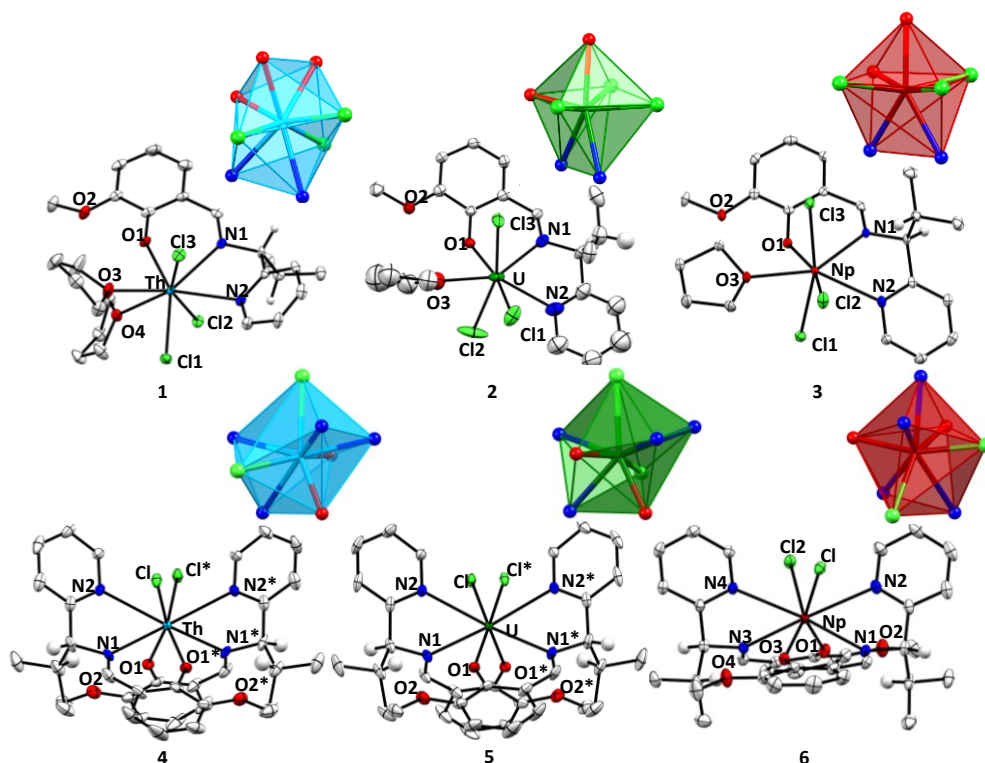


Figure 2. Ellipsoidal representation of complexes **1-6**. Ellipsoids are drawn at 30% probability level. The hydrogen atoms and lattice THF molecules are omitted for clarity. Inset: polyhedral representation of coordination environment around central metal ion.

Apart from that, change in the number of coordinating ligand to the various An^{4+} ions leads to differences in the alignment of the aromatic rings relative to the arbitrary plane comprising of An^{4+} , O_{Ph} , and $(H)C=N$ (Figures 3 and S13). In the solid-state structures of **1-3**, the aromatic rings are arranged in a pseudo-trans manner relative to the plane containing An^{4+} , O_{Ph} , and $(H)C=N$. While the phenoxide ring makes angles of 10.5° in **1**, 21.9° in **2** and 24.4° in **3** with the plane, the pyridyl ring is inclined by 36.1° , 38.9° , and 49.2° in **1**, **2**, and **3**, respectively (see Figure 3). With respect to the plane, the angle for the phenoxide and pyridyl rings increases in the order **3** > **2** > **1** suggesting increasingly constrained coordination with decreasing ionic radii. For complexes **4-6**, a change in the alignment of ligands with respect to the plane is seen. The complex appears to be

constrained in having two ligands in a manner that both the aromatic rings of a ligand are aligned on the same side of the plane. Interestingly, for complexes **4** and **5**, pyridyl and phenoxide rings are aligned with the horizontal plane in similar fashion (pyridyl 36.2° (**4**), 36.3° (**5**); phenoxide 7.8° (**4**), 7.9° (**5**)). Whereas, in complex **6**, pyridyl and phenoxide rings are inclined to angles of 34.1° and 25.1° w.r.t the plane. The maximum deviation w.r.t plane is observed in Np⁴⁺ complexes **3** and **6** potentially due to Np's smallest ionic radius among the three An⁴⁺ under investigation. This change in arrangement of the ligands depending on the size of the metal center once again highlights the considerable spatial flexibility of L^{Pr} in the complexes. This is in agreement with the observed slight differences between the solid-state structures, which may be affected by packing effects and weak intermolecular interactions, and the more symmetrical solution structure, which was suggested by our NMR results. In the end, we believe that An-Ligand coordination is comparatively relaxed and does not show considerable changes in the structural properties while changing the An⁴⁺ whereas coordination in the 2:1 complexes is comparatively strained and consequently exhibits greater structural rearrangements with small changes in ionic radii (0.02 Å from U⁴⁺ to Np⁴⁺) of An⁴⁺. [28]

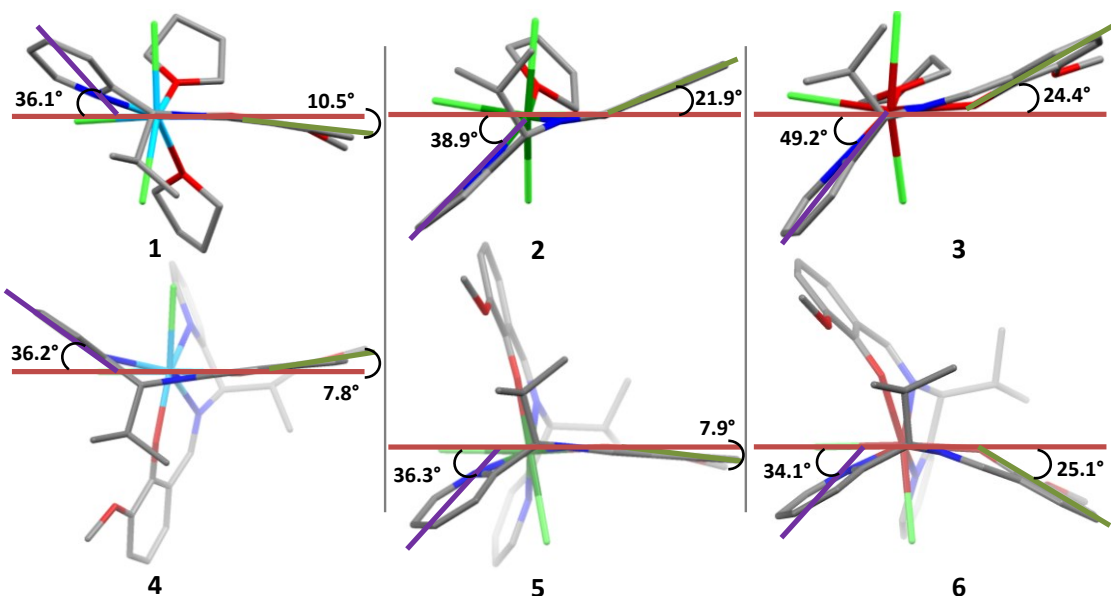


Figure 3. Capped stick representation of complexes **1-6**, displaying the angle formed by phenoxide ring (green line), pyridyl ring (magenta line) with the horizontal plane (brown line). The hydrogen atoms and lattice THF molecules are omitted for clarity.

Table 3. Selected bond distance (Å) parameters for complexes **1-6**.

Bond	1	2	3 ^a	4	5	6
An–O _{Ph}	2.199(4)	2.125(12)	2.122 (2)	2.235(2)	2.178(1)	2.167(1), 2.184(1)
An–N _{C=N}	2.673(5)	2.528(14)	2.514(2)	2.653(2)	2.606(1)	2.579(2), 2.615(2)
An–N _{Py}	2.725(5)	2.610(16)	2.559(2)	2.743(2)	2.720(1)	2.667(2), 2.669(2)
An–O _{THF}	2.543(5), 2.601(4)	2.455(16)	2.446(2)	-----	-----	----
An–Cl1	2.733(14)	2.635(5)	2.626(1)	2.766(7)	2.708(1)	2.681(1)
An–Cl2	2.709(14)	2.632(6)	2.629(1)	2.766(7)	2.708(1)	2.698(1)
An–Cl3	2.734(15)	2.662(5)	2.635(1)	----	----	----

^avalues are average of three molecular structures in the unit cell. Ionic radii (CN = 6): Th(IV) = 0.94 Å; U(IV) = 0.89 Å; Np(IV) = 0.87 Å.

Electrochemistry

To understand the redox properties of all synthesized compounds, cyclic voltammetry experiments were performed in acetonitrile solvent (Figures 4 and S14 and Table 4) and values are calculated vs $\text{Fc}^{0/+}$. [53] The free ligand **HL**^{Pr} exhibits three oxidative signals at, 0.47, 0.84, and 1.73 V vs $\text{Fc}^{0/+}$ and two reductive responses at 0.74 and 0.34 V vs $\text{Fc}^{0/+}$ (Figure S14). The oxidative responses at 0.47 V and 0.84 V are quasi-reversibly coupled with reductive responses at 0.34 V and 0.74 V, respectively. The $E_{1/2}$ values for these redox couples are 0.40 V and 0.79 V, respectively with peak-to-peak separations (ΔE_p) of 130 mV and 100 mV, respectively. Notably, the cathodic wave at 0.06 V (E_{pc}) and its anodic couple at 0.19 V (E_{pa}) are formed during the scan at the expense of features corresponding to both $E_{1/2}$'s. The reverse cycle exhibits the formation of an additional reductive response at -1.10 V potentially due to the reduction of a previously oxidized imine group but producing a chemically different species. The differential pulse voltammetry (DPV) experiment further confirms the presence of redox couples at 0.40 V, 0.76 V and 1.65 V.

Complex **1** displays a broad oxidative response (E_{pa}) at 0.86 V, 1.34 V, and 1.52 V along with an observable reductive couple (E_{pc}) at 0.75 V, 1.03 V and 1.44 V respectively, corresponding to ligand-based signals (Figure 4). The oxidative signals (E_{pa}) are positively shifted by ca. 390 mV and ca. 500 mV compared to the free ligand indicating an influence of the coordinated Th^{4+} in **1** on the ligand's oxidative potential. Moreover, cathodic waves (E_{pc}) at -0.92 V, -1.42 V and -1.69 V could be assigned to ligand-based signals due to potential formation of a C-C bond after ligand reduction. Such electrochemical behavior for An-(Schiff base) complexes was previously reported by Clément et. al. [36]. Interestingly, the bis-ligated Th(IV) complex **4** displays voltammogram similar to its 1:1 counterpart **1**. The two oxidative responses were observed at approximately 0.92 V and 1.20 V and four reductive responses at -1.40, -1.63, -2.12, and

–2.21 V. Since thorium is not expected to show any redox response within the potential range under discussion, these signals most likely corresponds to ligand-based responses.[54] We anticipate signals corresponding to Th(IV)/Th(III/II) beyond –2.3 V, [55,56] and thus not within the range of our experiments.

The U(IV) complex **2** exhibits five redox couples at $E_{1/2}$ = 0.45, 0.76, 0.98, 1.25, and 1.52 V on the positive side of voltammogram (Figure 4). While redox couples at $E_{1/2}$ = 0.76, 1.25, and 1.52 V best matches to ligand-based responses, the responses at $E_{1/2}$ = 0.45 V (E_{pa} = 0.49 V) and 0.98 V (E_{pa} = 1.05 V) could be tentatively assigned to metal-based U(IV)/U(V) and U(V)/U(VI) redox couples, respectively. Interestingly, ligand based oxidative responses (E_{pa}) at 0.82 V and 1.37 V are positively shifted by ca. 350 mV and 530 mV in comparison to **HL**^{Pr}. Moreover, similar to what was observed for complex **1** (E_{pc} = –1.68 V), a ligand-based reductive feature at –1.76 V (E_{pc}) is observed in **2**. Whereas the feature at –2.09 V most likely corresponds to a U(IV)/U(III) reductive process. [33] On the other hand, the 2:1 U(IV) complex **5** exhibits four prominent oxidative features at E_{pa} = 0.73, 1.18, 1.61, and 1.86 V along with the four noticeable reductive responses at E_{pc} = –1.22, –1.89, –2.05, and –2.22 V. The oxidative features at 0.73, 1.61 and 1.86 V correlate to ligand-based responses. However, in contrast to observations of two metal-centered oxidative responses in **2**, only one oxidative feature at 1.18 V is observed in **5** which we tentatively assigned as U(IV)/U(V/VI). In addition, reductive features at E_{pc} = –1.22, –1.89 and –2.22 V [33] correspond to ligand-based responses, whereas the feature at –2.05 V could be assigned to a U(IV)/U(III) response.

For complex **3**, broad oxidative (E_{pa}) and reductive signals (E_{pc}) indicating that metal-based responses have closely matched potentials with that of ligand. However, a closer look at the voltammogram shows the presence of four oxidative responses 0.97 V, 1.05 V, 1.28 V, and

1.71 V. In addition, a weak signal at approx. 0.78 V is observed. Oxidative responses at 0.97 V, 1.28 V, and 1.71 V are closely matched with the ligand-based responses in complexes **1** and **2**, whereas signals at approx. 0.78 V and 1.05 V could be tentatively assigned as Np(IV)/Np(V) and Np(V)/Np(VI) processes, respectively. Importantly, ligand-based signals at $E_{pa} = 0.97$ V and 1.28 V are positively shifted by 500 mV and 440 mV, respectively, in comparison to the free ligand, and are similar to those of complexes **1** and **2** containing Th^{4+} and U^{4+} ions. The reductive responses at the negative side of voltammogram could be assigned as ligand-based responses. Based on one reference available in the literature, we anticipate the observation of Np(IV) based reduction responses beyond our analytical range of -2.5 V.[57]. On the other hand, the 2:1 counterpart **6** displays broad oxidative signals, similar to **3**, having four measurable features at 0.79, 1.21, 1.46, and 1.92 V along with a weak trace at 0.64 V. Considering our observation in other complexes (**1-5**), we tentatively assign 0.89, 1.46 and 1.92 V to the ligand-based responses, whereas, features at 0.64 V and 1.21 V could be assigned as Np(IV)/Np(V) and Np(V)/Np(VI) responses, respectively. Moreover, four reductive responses at $E_{pc} = -1.07, -1.90, -2.04$ and -2.30 V could be assigned to ligand-based responses. Gratifyingly, DPV experiments further corroborate the observations for these complexes.

Table 4. Redox potentials values for **HL^{pr}** and complexes **1-6** determined by CV.

Entry	Ligand-based				Metal-based			
	E_{pa}	E_{pc}	$E_{1/2}$	DPV	E_{pa}	E_{pc}	$E_{1/2}$	DPV
HL^{pr}	0.47, 0.84, 1.73	0.34, 0.74	0.40, 0.79	0.40, 0.76, 1.65	----	----	----	----
1^a	0.86, 1.34, 1.52	0.75, 1.03, 1.44, -0.92, -1.37, -1.68	0.80, 1.18	0.70, 1.09, 1.44, -0.75, -1.09	----	> 2.1	----	----
2	0.82, 1.37, 1.59	0.71, 1.13, 1.45, -1.76	0.76, 1.25, 1.52	0.76, 1.24, 1.45, -1.70	0.49, 1.05	0.42, 0.91, -2.09	0.45, 0.98	0.44, 0.98, -2.02
3	0.97, 1.28, 1.71	-0.89, -1.21	-----	0.89, 1.22, 1.46	0.78, 1.05	-1.47, -1.90, -2.40	-----	0.51, 0.77, -1.44, -1.85, -2.39
4	0.92, 1.20	-1.40, -1.63, -2.21	-----	0.77, 1.03, 2.05, -1.31, -2.00, -2.60	----	----	----	-2.14
5	0.73, 1.61, 1.86	1.40, -1.22, -1.89, -2.22	----	0.67, 1.07, 1.59, 1.78, -1.86, -1.81, -2.19	1.18	-2.05	----	-1.90
6	0.89, 1.46, 1.92	-1.07, -1.90, -2.30		0.83, 1.05, 1.19, 1.36, 1.82, - 1.03, -2.25	0.64, 1.21	-2.04	----	-1.99

^a values could not be assigned exactly.

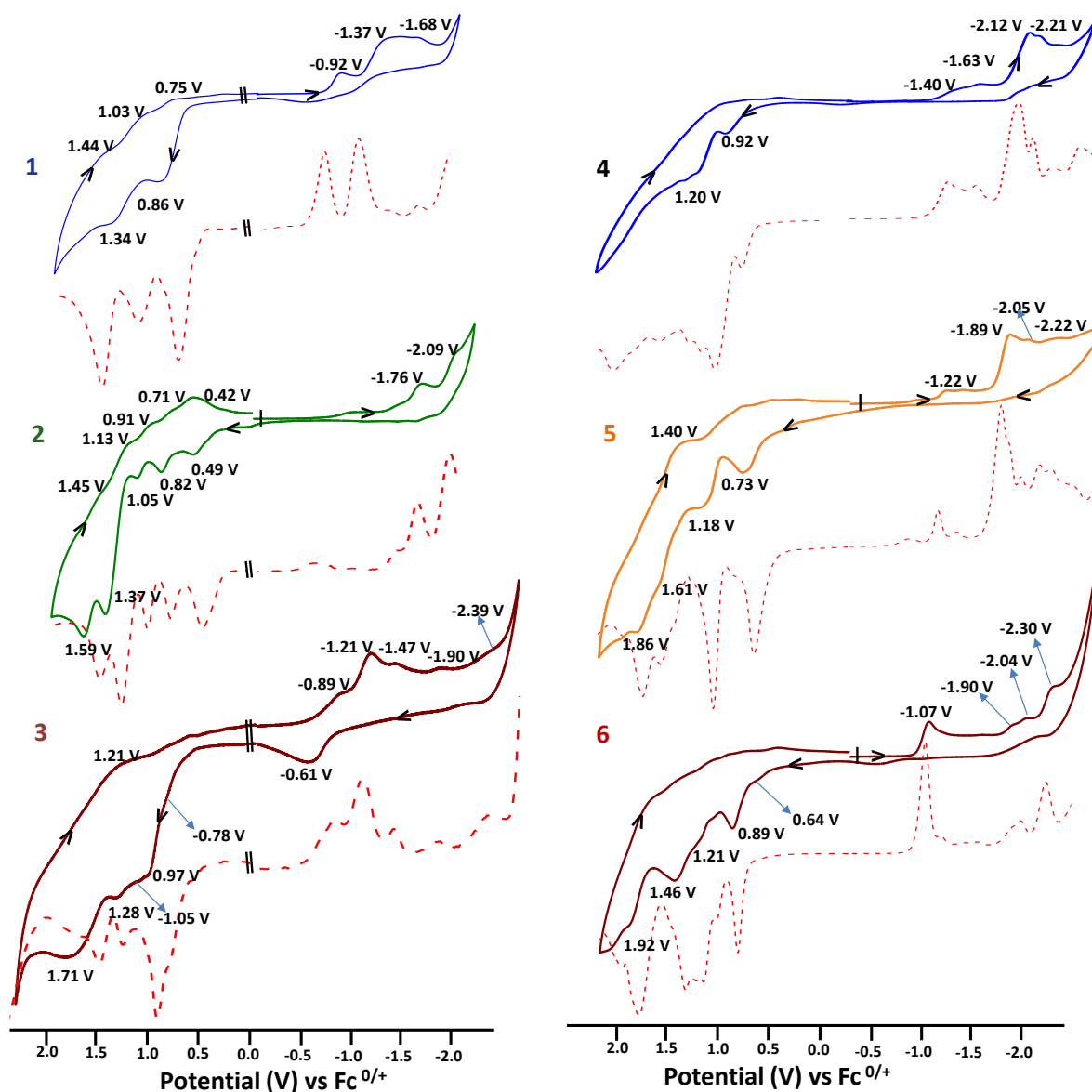


Figure 4. Cyclic (thick line) and Differential Pulse (dotted line) voltammogram of 1:1 complexes **1** (—), **2**(—) and **3** (—) and 2:1 complexes **4** (—), **5**(—) and **6** (—) vs $\text{Fc}^{0/+}$ in acetonitrile solvent. Conditions: Ligand/complex approx. 1 mM, $\text{n-Bu}_4\text{NPF}_6$, supporting electrolyte approx. 100 mM, glassy carbon working electrode, Pt wire auxiliary electrode, Ag/Ag^+ reference electrode; scan rate: 100 mV s^{-1} .

431 Binding Studies

432 We performed concentration dependent absorption titrations to understand the binding affinity of
433 (L^{Pr})⁻ with different metal ions (Figures S15-S17). In complex **1-3**, absorption spectral titration
434 between Th⁴⁺, U⁴⁺, and Np⁴⁺ with (L^{Pr})¹⁻ exhibited an increase in absorption feature at 450 nm.
435 The changes in the absorbance reached maxima on addition of 1.0 equiv. metal ion indicating a 1:1
436 stoichiometry of (L^{Pr})⁻ with respect to the actinide ion, in agreement with the SC-XRD results.
437 The binding coefficients were calculated (at 450 nm for **1-3**) using the Benesi–Hildebrand eq. 1.
438 [58-60]

$$439 \quad \frac{1}{(A - A_0)} = \frac{1}{K(A_{\max} - A_0)[An^{n+}]^x} + \frac{1}{(A_{\max} - A_0)} \quad (1)$$

440 Here, 'A₀' is the absorbance of the ligand (L^{Pr})⁻, 'A' is the change in absorbance after addition
441 of An ions, 'A_{max}' is the absorbance value after adding excess amount of An ions, 'K' is the
442 association constant (M⁻¹), [Anⁿ⁺] is the concentration of the An ions added (M), and 'x' is the no.
443 of equivalents. The linear regression plot between absorption intensity, 1/[A-A₀] vs 1/[Anⁿ⁺]^x
444 varied linearly as a function of 1/[Anⁿ⁺] (x = 1), confirming a 1:1 stoichiometry (Figures S15-S17).
445 The binding constants (K) were calculated as (2.3 ± 0.4) × 10³ M⁻¹ for **1**, (1.54 ± 0.3) × 10³ M⁻¹ for
446 **2**, and (2.01 ± 0.4) × 10² M⁻¹ for **3**. These numbers suggest that Th⁴⁺ and U⁴⁺ have similar binding
447 affinities to (L^{Pr})⁻ whereas Np⁴⁺ has an approx. ten-fold weaker binding affinity.

448 Conclusions

449 Herein we report the synthesis and characterization of six mono-nuclear tetravalent actinide
450 complexes (**1-6**) comprising mono-ligated (**1-3**) and bis-ligated complexes (**4-6**) with a novel
451 Schiff base-type ligand. Their comparative analysis exhibits the influence of change in

coordination environment on the (electro-)chemical properties of actinide complexes. Notably, the effect of the actinide on the electronic properties of the complexes is more pronounced in the 1:1 complexes than for their 2:1 counterparts. This is most obvious in NMR spectroscopy, where ^1H NMR for 1:1 Th(IV) complex (**1**) is shifted upfield from its 2:1 counterpart **4** and ^1H NMR signals for 1:1 U(IV) and Np(IV) complexes are highly paramagnetically shifted between -70 to 40 ppm. These signals appeared within -35 to 25 ppm for 2:1 complexes **5** and **6**. Single crystal structures reveal an increase in the An-ligand bond distances when moving from 1:1 to 2:1 stoichiometry, which also confirms our interpretation of NMR data as indicating weak An-ligand interactions in 2:1 complexes. Apart from that, bond distances in both 1:1 or 2:1 complex decrease with the decreasing ionic radii of An(IV) center while traversing the An series. These structural changes are accompanied by changes in the arrangement of the aromatic rings in the complexes, which emphasizes the limited structural flexibility in this system. The maximum deviation of phenoxide and pyridyl ring(s) is observed in Np^{4+} complexes **3** and **6**. This goes along with binding studies suggesting that Np^{4+} has a significantly weaker binding affinity to $(\text{L}^{\text{Pr}})^-$ than Th^{4+} and U^{4+} . Cyclic voltammetry studies revealed an increase in the ligand-based oxidation potential by 200 - 300 mV in all the complexes. In addition, several redox transitions could be tentatively assigned to actinide reductions and oxidations. While these processes need to be verified, cyclic voltammetry suggests $(\text{L}^{\text{Pr}})^-$ may be suitable to stabilize actinides in both low and high oxidation states. Our results add to the very limited database of structures of actinide-organic complexes and sheds new light on the interplay of molecular and electronic structure in these compounds.

473 **Supporting Information.**

474 The Supporting Information is available free of charge at XXXXXXXXXX.

- 475 • Additional details related to NMR, UV-vis, FTIR and crystal refinement parameters for all
476 the synthesized molecules.

477 **Accession Codes**

478 CCDC 2075052-2075054 for complexes **1-3** and 2152165-2152167 for complexes **4-6** contain the
479 supplementary crystallographic data for this paper. These data can be obtained free of charge via
480 www.ccdc.cam.ac.uk/data_request/cif, or by emailing data_request@ccdc.cam.ac.uk, or by
481 contacting The Cambridge Crystallographic Data Centre, 12 Union Road, Cambridge CB2 1EZ,
482 UK; fax: +44 1223 336033.

483 **Corresponding Author**

484 * Helmholtz-Zentrum Dresden-Rossendorf (HZDR), Institute of Resource Ecology, Bautzner
485 Landstraße 400, 01328 Dresden, Germany.

486 Email : Moritz.schmidt@hzdr.de

487 **Notes**

488 The authors declare no competing financial interest.

489 **ACKNOWLEDGMENT**

490 DB thanks Sebastian Fischer and Kuldeep Mahiya for crystallographic help and Luisa Köhler for
491 support during experimental work.

492 **REFERENCES**

- 493 1. Götzke, L.; Schaper, G.; März, J.; Kaden, P.; Huittinen, N.; Stumpf, T.; Kammerlander, K.
494 K.K.; Brunner, E.; Hahn, P.; Mehnert, A.; Kersting, B.; Henle, T.; Lindoy, L. F.; Zandoni, G.;
495 Weigand, J. J. Coordination chemistry of f-block metal ions with ligands bearing bio-relevant
496 functional groups. *Coord. Chem. Rev.* **2019**, *386*, 267–309.
- 497 2. Lv, K.; Fichter, S.; Gu, M.; März, J.; Schmidt, M. An updated status and trends in actinide
498 metal-organic frameworks (An-MOFs): From synthesis to application. *Coord. Chem. Rev.*
499 **2021**, *446*, 214011.
- 500 3. Yoshimura, T.; Nakaguchi, M.; Morimoto, K. Synthesis, Structures, and Proton Self-Exchange
501 Reaction of μ_3 -Oxido/Hydroxido Bridged Trinuclear Uranyl(VI) Complexes with Tridentate
502 Schiff-Base Ligands. *Inorg. Chem.* **2017**, *56*, 4057-4064.
- 503 4. Camp, C.; Mougél, V.; Horeglad, P.; Pecaut, J.; Mazzanti, M. Multielectron Redox
504 Reactions Involving C–C Coupling and Cleavage in Uranium Schiff Base
505 Complexes. *J. Am. Chem. Soc.* **2010**, *132*, 17374–17377.
- 506 5. Camp, C.; Andrez, J.; Pecaut, J.; Mazzanti, M. Synthesis of electron-rich uranium (IV)
507 complexes supported by tridentate Schiff base ligands and their multi-electron redox chemistry.
508 *Inorg. Chem.* **2013**, *52*, 7078–7086.
- 509 6. Camp, C.; Chatelain, L.; Mougél, V.; Pecaut, J.; Mazzanti, M. Ferrocene-based tetradentate
510 Schiff bases as supporting ligands in uranium chemistry. *Inorg. Chem.* **2015**, *54*, 5774–5783.
- 511 7. Hayton, T. W.; Wu, G. Synthesis, Characterization, and Reactivity of a Uranyl β -Diketiminato
512 Complex. *J. Am. Chem. Soc.* **2008**, *130*, 2005-2014.

- 513 8. Castro-Rodriguez, I.; Nakai, H.; Zakharov, L. N.; Rheingold, A. L.; Meyer, K. A Linear, O-
514 Coordinated η^1 -CO₂ Bound to Uranium. *Science* **2004**, *305*, 1757–1759.
- 515 9. Evans, W. J.; Kozimor, S. A.; Ziller, J. W. Molecular octa-uranium rings with alternating nitride
516 and azide bridges. *Science* **2005**, *309*, 1835–1838.
- 517 10. Summerscales, O. T.; Cloke, F. G. N.; Hitchcock, P. B.; Green, J. C.; Hazari, N. Reductive
518 cyclotrimerization of carbon monoxide to the deltate dianion by an organometallic uranium
519 complex. *Science* **2006**, *311*, 829–831.
- 520 11. Mansell, S. M.; Kaltsoyannis, N.; Arnold, P. L. Small Molecule Activation by Uranium
521 Tris(aryloxides): Experimental and Computational Studies of Binding of N₂, Coupling of CO,
522 and Deoxygenation Insertion of CO₂ under Ambient Conditions. *J. Am. Chem. Soc.* **2011**, *133*,
523 9036–9051.
- 524 12. Diaconescu, P. L. Reactions of Aromatic N-Heterocycles with d⁰fn-Metal Alkyl Complexes
525 Supported by Chelating Diamide Ligands. *Acc. Chem. Res.* **2010**, *43*, 1352–1363.
- 526 13. Wang, J.; Gurevich, Y.; Botoshansky, M.; Eisen, M. S. Unique σ -Bond Metathesis of
527 Silylalkynes Promoted by an ansa-Dimethylsilyl and Oxo-Bridged Uranium Metallocene. *J.*
528 *Am. Chem. Soc.* **2006**, *128*, 9350–9351
- 529 14. Fox, A. R.; Bart, S. C.; Meyer, K.; Cummins, C. C. Towards uranium catalysts. *Nature* **2008**,
530 *455*, 341–349.
- 531 15. Arnold, P. L.; Love, J. B.; Patel, D. Pentavalent uranyl complexes. *Coord. Chem. Rev.* **2009**,
532 *253*, 1973–1978.

- 533 16. Fortier, S.; Hayton, T. W. Oxo ligand functionalization in the uranyl ion (UO_2^{2+}). *Coord. Chem.*
534 *Rev.* **2010**, *254*, 197-214.
- 535 17. Wang, K. -X.; Chen, J. -S. Extended structures and physicochemical properties of uranyl–
536 organic compounds. *Acc. Chem. Res.* **2011**, *44*, 531–540.
- 537 18. Andrews, M. B.; Cahill, C. L. Uranyl bearing hybrid materials: synthesis, speciation, and solid-
538 state structures. *Chem. Rev.* **2013**, *113*, 1121–1136.
- 539 19. Thuéry, P.; Harrowfield, J. Cavity Formation in Uranyl Ion Complexes with Kemp's
540 Tricarboxylate: Grooved Diperic Nets and Polynuclear Cages. *Inorg. Chem.* **2021**, *60*,
541 1683–1697.
- 542 20. Cowie, B. E.; Purkis, J. M.; Austin, J.; Love, J. B.; Arnold, P. L. Thermal and Photochemical
543 Reduction and Functionalization Chemistry of the Uranyl Dication, $[\text{U}^{\text{VI}}\text{O}_2]^{2+}$. *Chem. Rev.*
544 **2019**, *119*, 10595–10637.
- 545 21. Sessler, J. L.; Melfi, P. J.; Pantos, G. D. Uranium complexes of multidentate N-donor ligands.
546 *Coord. Chem. Rev.* **2006**, *250*, 816–843.
- 547 22. Jori, N.; Falcone, M.; Scopelliti, R.; Mazzanti, M. Carbon Dioxide Reduction by Multimetallic
548 Uranium (IV) Complexes Supported by Redox-Active Schiff Base Ligands. *Organometallics*,
549 **2020**, *39*, 1590–1601.
- 550 23. Wang, S.; Li, T.; Heng, Y.; Wang, D.; Hou, G.; Zi, G.; Walter, M. D. Small-Molecule
551 Activation Mediated by $[\eta^5\text{-1,3-(Me}_3\text{Si)}_2\text{C}_5\text{H}_3]_2\text{U(bipy)}$.
552 <https://doi.org/10.1021/acs.inorgchem.2c00423>,

- 553 24. Hsueh, F. -C.; Barluzzi, L.; Keener, M.; Rajeshkumar, T.; Maron, L.; Scopelliti, R.; Mazzanti,
554 M. Reactivity of Multimetallic Thorium Nitrides Generated by Reduction of Thorium Azides.
555 *J. Am. Chem. Soc.* **2022**, *144*, 3222–3232.
- 556 25. Makarov, K.; Kaushansky, A.; Eisen, M. S. Catalytic Hydroboration of Esters by Versatile
557 Thorium and Uranium Amide Complexes. *ACS Catal.* **2022**, *12*, 273–284.
- 558 26. Schelter, E. J.; Yang, P.; Scott, B. L.; Thompson, J. D.; Martin, R. L.; Hay, P. J.; Morris, D. E.;
559 Kiplinger, J. L. Systematic studies of early actinide complexes: Uranium (IV) fluoroketimides.
560 *Inorg. Chem.* **2007**, *46*, 7477–7488.
- 561 27. Ephritikhine, M. Recent advances in organoactinide chemistry as exemplified by
562 cyclopentadienyl compounds. *Organometallics*, **2013**, *32*, 2464–2488.
- 563 28. Köhler, L.; Patzschke, M.; Schmidt, M.; Stumpf, T.; März, J. How 5 f Electron Polarisability
564 Drives Covalency and Selectivity in Actinide N-Donor Complexes. *Chem. Eur. J.* **2021**, *27*,
565 18058-18065.
- 566 29. Radoske, T.; März, J.; Patzschke, M.; Kaden, P.; Walter, O.; Schmidt, M.; Stumpf, T., Bonding
567 Trends in Tetravalent Th–Pu Monosalen Complexes, *Chem. Eur. J.* **2020**, *26*, 16853-16859.
- 568 30. Radoske, T.; Kloditz, R.; Fichter, S.; März, J.; Kaden, P.; Patzschke, M.; Schmidt, M.; Stumpf,
569 T.; Walter, O.; Ikeda, A. Systematic comparison of the structure of homoleptic tetradentate
570 N₂O₂-type Schiff base complexes of tetravalent f-elements (M(IV) = Ce, Th, U, Np, and Pu) in
571 solid state and in solution. *Dalton Trans.* **2020**, *49*, 17559-17570.

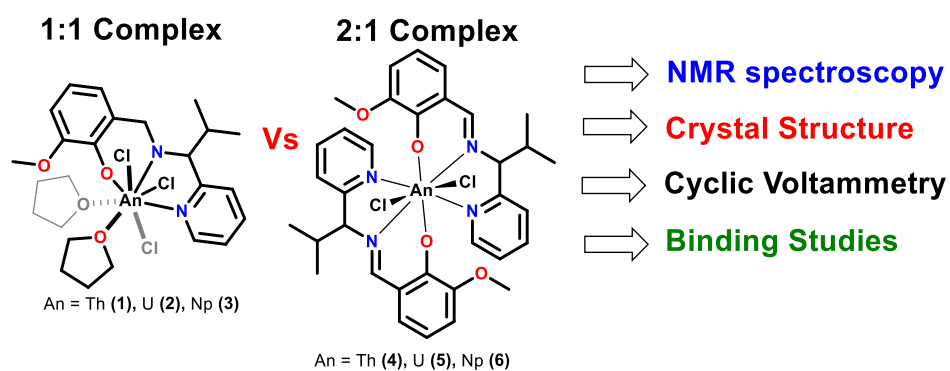
- 572 31. Klammm, B. E.; Windorff, C. J.; Celis-Barros, C.; Marsh, M. L.; Meeker, D. S.; Albrecht-
573 Schmitt, T. E. Experimental and Theoretical Comparison of Transition-Metal and Actinide
574 Tetravalent Schiff Base Coordination Complexes. *Inorg. Chem.* **2018**, *57*, 15389–15398.
- 575 32. Stobbe, B. C.; Powell, D. R.; Thomson, R. K. Schiff base thorium (IV) and uranium (IV) chloro
576 complexes: synthesis, substitution and oxidation chemistry. *Dalton Trans.* **2017**, *46*, 4888-
577 4892.
- 578 33. Dame, A. N.; Bharara, M. S.; Barnes, C. L.; Walensky, J. R. Synthesis of Thorium(IV) and
579 Uranium(IV) Salicylaldiminate Pseudo-Halide Complexes. *Eur. J. Inorg. Chem.* **2015**, 2996–
580 3005 and references cited therein.
- 581 34. Brasse, M.; Cámpora, J.; Palma, P.; Álvarez, E.; Cruz, V.; Ramos, J.; Reyes, L. Nickel 2-
582 Iminopyridine N-Oxide (PymNox) Complexes: Cationic Counterparts of Salicylaldiminate-
583 Based Neutral Ethylene Polymerization Catalysts, *Organometallics*, **2008**, *27*, 4711–4723.
- 584 35. Axenov, K. V.; Klinga, M.; Lehtonen, O.; Koskela, H. T.; Leskelä, M.; Repo, T. Hafnium
585 Bis(phenoxyimino) Dibenzyl Complexes and Their Activation toward Olefin Polymerization.
586 *Organometallics*, **2007**, *26*, 1444 –1460.
- 587 36. Camp, C.; Andrez, J.; Pécaut, J.; Mazzanti, M. Synthesis of Electron-Rich Uranium(IV)
588 Complexes Supported by Tridentate Schiff Base Ligands and Their Multi-Electron Redox
589 Chemistry. *Inorg. Chem.* **2013**, *52*, 7078–7086.
- 590 37. Swayer, D. T.; Roberts, J. L. Experimental Electrochemistry for Chemists, Wiley, New York,
591 **1974**.

- 592 38. Connelly, N. G.; Geiger, W. E. Chemical redox agents for organometallic chemistry. *Chem.*
593 *Rev.* **1996**, *96*, 877-910.
- 594 39. Bruker, Vol. v2016.9-0, Bruker AXS Inc., Madison, Wisconsin, USA., **2016**.
- 595 40. Sheldrick, G. M. University of Göttingen, Germany, **1996**.
- 596 41. Sheldrick, G. M. *Acta Cryst.* **2015**, *A71*, 3-8.
- 597 42. Sheldrick, G. M. *Acta Crystallogr. Sect. A*, **2008**, *64*, 112-122.
- 598 43. Farrugia, L. J. WinGX, version 1.64, An integrated system of Windows Programs for the
599 Solution, Refinement and Analysis of Single- Crystal X-ray Diffraction Data, Department of
600 Chemistry, University of Glasgow, **2003**.
- 601 44. Spek, A. L. PLATON, A Multipurpose Crystallographic Tool, version 21116, Utrecht
602 University, The Netherlands.
- 603 45. Fichter, S.; Kaufmann, S.; Kaden, P.; Brunner, T. S.; Stumpf, T.; Roesky, P. W.; März, J.
604 Enantiomerically Pure Tetravalent Neptunium Amidinates: Synthesis and Characterization.
605 *Chem. Eur. J.* **2020**, *26*, 8867–8870.
- 606 46. Rüede J. E.; Thornton, D. A. The Far Infrared Spectra of Metal Chloride Complexes of Pyridine
607 on Relation to their Structures, *J. Mol. Str.*, **1976**, *34*, 75-81.
- 608 47. Herath, I. D.; Breen, C.; Hewitt, S. H.; Berki, T. R.; Kassir, A. F.; Dodson, C.; Judd, M.; Jabar,
609 S.; Cox, N.; Otting, G.; Butler, S. J. A Chiral Lanthanide Tag for Stable and Rigid Attachment
610 to Single Cysteine Residues in Proteins for NMR, EPR and Time-Resolved Luminescence
611 Studies. *Chem. Eur. J.* **2021**, *27*, 13009–13023.

- 612 48. Otting, G. Protein NMR Using Paramagnetic Ions. *Annu. Rev. Biophys.* **2010**, 39, 387-405.
- 613 49. Nitsche, C.; Otting, G. NMR studies of ligand binding. *Cur. Op. Str. Bio.* **2018**, 48,16–22.
- 614 50. Better resolved COSY NMRs from U(IV) complexes **2** and **5** are used for proton assignment in
615 paramagnetic NMR. Moreover, Np(IV) complexes exhibit spectrum like U(IV) and therefore,
616 signals are assigned in the identical manner.
- 617 51. Harnden, A. C.; Suturina, E. A.; Batsanov, A. S.; Senanayake, P. K.; Fox, M. A.; Mason, K.;
618 Vonci, M.; McInnes, E. J. L.; Chilton, N. F.; Parker, D. Unravelling the Complexities of
619 Pseudocontact Shift Analysis in Lanthanide Coordination Complexes of Differing Symmetry.
620 *Angew. Chem., Int. Ed.* **2019**, 131, 10396-10400.
- 621 52. Alvarez, S. Continuous Shape Measures Study of the Coordination Spheres of Actinide
622 Complexes – Part 1: Low Coordination Numbers. *Eur. J. Inorg.Chem.* **2021**, 3632–3647
- 623 53. Cyclic voltammogram for 1:1 complexes (**1-3**) were found unstable for full cycle having both
624 oxidation and reduction regions. Therefore, both reduction and oxidation features are measured
625 independently. Whereas 2:1 complexes (**4-6**) display stable cyclic voltammogram for at least
626 one full cycle of measurement. Notably, though we have observed electronic influence of
627 chirality only in Th(IV) complexes **1** and **4**. We believe that the redox signals contain responses
628 from at least two An complex species for 1:1 complexes and two or more An complex species
629 for 2:1 complex due to the presence of ligand having mixture of both ‘R and S’ the configuration
630 at chiral ‘C8’ center.

- 631 54. Ward, A. L.; Buckley, H. L.; Lukens, W. W.; Arnold, J. Synthesis and Characterization of
632 Thorium(IV) and Uranium(IV) Corrole Complexes. *J. Am. Chem. Soc.* **2013**, *135*, 13965–
633 13971.
- 634 55. Wedal, J. C.; Barlow, J. M.; Ziller, J. W.; Yang, J. Y.; Evans, W. J. Electrochemical studies of
635 tris(cyclopentadienyl)thorium and uranium complexes in the +2, +3, and +4 oxidation states.
636 *Chem. Sci.* **2021**, *12*, 8501-8511.
- 637 56. Inman, C. J.; Geoffrey, F.; Cloke, N. The experimental determination of Th(IV)/Th(III) redox
638 potentials in organometallic thorium complexes, *Dalton Trans.* **2019**, *48*, 10782-10784.
- 639 57. Klamm, B. E.; Windorff, C. J.; Celis-Barros, C.; Beltran-Leiva, M. J.; Sperling, J. M.; Albrecht-
640 Schöznart, T. E. Exploring the Oxidation States of Neptunium with Schiff Base Coordination
641 Complexes, *Inorg. Chem.* **2020**, *59*, 18035–18047
- 642 58. Benesi, H. A.; Hildebrand, J. H. A spectrophotometric investigation of the interaction of iodine
643 with aromatic hydrocarbons, *J. Am. Chem. Soc.* **1949**, *71*, 2703-2707.
- 644 59. Bansal, D.; Kumar, G.; Hundal, G.; Gupta, R. Mononuclear complexes of amide-based ligands
645 containing appended functional groups: role of secondary coordination spheres on catalysis.
646 *Dalton Trans.* **2014**, *43*, 14865-14875.
- 647 60. Bansal, D.; Gupta, R. Chemosensors containing appended benzothiazole group(s): selective
648 binding of Cu²⁺ and Zn²⁺ ions by two related receptors. *Dalton Trans.* **2016**, *45*, 502-507.
- 649

650 **SYNOPSIS.** A series of mononuclear tetravalent actinide complexes (**1-6**) have been synthesized
651 using a new monoanionic Schiff base ligand (**HL^{Pr}**). Comparative analysis between 1:1 complexes
652 [$\text{MCl}_3\text{-L}^{\text{Pr}}\cdot n\text{THF}$] (**1-3**) and 2:1 complexes [$\text{MCl}_2\text{-L}^{\text{Pr}}_2$] (**4-6**) shows intriguing influence of
653 coordinating ligands in coalescence with coordinating properties of An^{4+} centers on the spectral,
654 structural and electrochemical properties.



655